X-ray processing of a realistic ice mantle can explain the gas abundances in protoplanetary disks

Angela Ciaravella[a,1], Guillermo M. Muñoz Caro[b], Antonio Jiménez-Escobar[a], Cesare Cecchi-Pestellini[a], Li-Chieh Hsiao[c], Chao-Hui Huang[c], and Yu-Jung Chen[c,1]

[a]Osservatorio Astronomico di Palermo, Istituto Nazionale di Astrofisica, 90134 Palermo, Italy; [b]Centro de Astrobiología, Consejo Superior de Investigaciones Científicas - Instituto Nacional de Técnica Aeroespacial, 28850 Torrejón de Ardoz, Madrid, Spain; and [c]Department of Physics, National Central University, Jhongli 32054, Taiwan

Edited by Neta A. Bahcall, Princeton University, Princeton, NJ, and approved June 1, 2020 (received for review March 19, 2020)

The Atacama Large Millimeter Array has allowed a detailed observation of molecules in protoplanetary disks, which can evolve toward solar systems like our own. While CO, CO_2, HCO, and H_2CO are often abundant species in the cold zones of the disk, CH_3OH or CH_3CN are only found in a few regions, and more-complex organic molecules are not observed. We simulate, experimentally, ice processing in disks under realistic conditions, that is, layered ices irradiated by soft X-rays. X-ray emission from young solar-type stars is thousands of times brighter than that of today's sun. The ice mantle is composed of a H_2O:CH_4:NH_3 mixture, covered by a layer made of CH_3OH and CO. The photoproducts found desorbing from both ice layers to the gas phase during the irradiation converge with those detected in higher abundances in the gas phase of protoplanetary disks, providing important insights on the nonthermal processes that drive the chemistry in these objects.

astrochemistry | protoplanetary disks | X-rays | methods: laboratory: molecular

Ice mantles covering (sub)micron dust grains in interstellar and protoplanetary environments are mainly composed of simple species in a water-dominated ice. Hydrogenation of O, C, and N on the grain surface produces a first layer of water (H_2O), methane (CH_4), ammonia (NH_3), and other reduced species. On top of this, there is a second layer of species that are formed in the gas phase and require lower temperatures to stick onto the dust, with carbon monoxide (CO) being the most abundant component (1–3). The coalescence of CO with methanol (CH_3OH) in these ices is inferred from the fit of the CO ice band profile near 4.6 micron observed in the infrared (4). The hydrogenation of CO molecules in these ices is proposed as a plausible formation mechanism for CH_3OH (5). Most experimental simulations of astrophysical ice processing with an energy source were conducted with either pure or binary ice analogs to understand the photolysis and radiolysis of molecules and the product formation (6). Multicomponent ice mixtures were also explored to mimick the formation of complex organic molecules (COMs) in the ice, in particular, those remaining in the residue at room temperature after warm-up of ultraviolet or ion-processed ices. Since amino acids, sugars, nucleobases, and other prebiotic species are among the products of ice irradiation, these studies are of interest to a broad scientific community (7–11). More recently, COMs were also produced as the result of X-ray irradiation of ice analog mixtures (12, 13).

Here we report an experimental simulation of a more astrophysically realistic ice mantle morphology, organized in a bilayered structure of segregated polar and apolar components (14, 15). The selected relative abundances of the ice species are similar to previous experimental works dedicated to ultraviolet irradiation of ice mixtures (10, 16, 17), but none of these works segregated the molecular species into distinct polar and apolar ice layers. This ice composition was inferred from astronomical observations (3), and it is closer to the abundances found around protostellar sources (18, 19). Indeed, the line of sight abundances of CH_3OH and CO_2 are about 5 to 10 times lower than the abundances found close to the protostellar sources, due to the prevalence of H_2O ice in the cold outer regions (18). Specifically, the ice sample presented in this paper is composed of a H_2O:CH_4:NH_3 (2:1:1) mixture, coated with a layer of mixed CO and CH_3OH (3:1), and exposed to soft X-rays. We note that a higher relative abundance of H_2O in the ice, similar to the median values in astronomical observations (3), leads to a more efficient formation of ultraviolet photoproducts (16, 20), but this composition is expected to be less representative of the ice found near the protostar, where X-rays permeate the ice.

Because ultraviolet photons have a penetration of a few hundred monolayers in the ice, where a monolayer corresponds to the thickness of one molecule and a column density of about 10^{15} molecules per cm^2, the present mantle configuration is very suitable to the deeply penetrating soft X-rays, allowing study in detail of the formation, and eventual photodesorption, of radiolysis products. In the ice mixtures studied to date (12, 13, 21), the identified X-ray products are common to the ultraviolet experiments. The main focus of this work is, therefore, to follow the destruction of the original ice components, the formation of products in the realistic ice analogs, and their release into the gas phase. Particular attention is paid to the desorption of molecules during the irradiation, since this allows comparison with the recent observations of protoplanetary disks using

Significance

Of the over 200 molecules observed in the tenuous gas filling the space between stars, many are organic. Such species mostly form in simple molecular ices coating dust grains in dark interstellar regions. Understanding the production of organics in the early stages of star formation is critical to tracing the evolution from simple molecules to potentially life-bearing chemistry. Laboratory experiments have shown that a complex chemistry can originate in ices. We experimentally studied the formation and ejection into the gas phase of organics in ice analogues irradiated by X-rays, obtaining results in close agreement with ALMA observations of protoplanetary disks. X-rays from young solar-type stars are thousands of times higher than today's sun, with chemical implications, so far, relatively unexplored.

Author contributions: A.C., G.M.M.C., A.J.-E., C.C.-P., L.-C.H., C.-H.H., and Y.-J.C. performed research; A.C., G.M.M.C., A.J.-E., C.C.-P., L.-C.H., C.-H.H., and Y.-J.C. analyzed data; and A.C., G.M.M.C., A.J.-E., C.C.-P., L.-C.H., and Y.-J.C. wrote the paper.

The authors declare no competing interest.

This article is a PNAS Direct Submission.

Infrared and mass spectra data used in this paper are available at Harvard Dataverse, https://dataverse.harvard.edu (DOI: 10.7910/DVN/TMB6AF).

[1]To whom correspondence may be addressed. Email: angela.ciaravella@inaf.it or asperchen@phy.ncu.edu.tw.

First published June 30, 2020.

the Atacama Large Millimeter Array (ALMA). Young solar-type stars are powerful sources of X-rays, thousands of times brighter than our middle-aged sun ($\sim 10^{27}$ erg·s^{-1}), with chemical implications on the surrounding disks so far relatively unexplored. X-ray emission in such stars fades with age but overcomes the extreme ultraviolet emission up to 1 Gyr (22), and penetrates the disk up to larger distances. X-rays emitted by a typical T Tauri star propagate near the denser region of the disk midplane well beyond 10 AU and the CO snowline, where the ultraviolet radiation is inhibited (23). Thus, X-rays cover a larger temperature gradient and a broader grain size distribution up to a few micron-sized dust particles. ALMA allows the detailed observation of various molecules in the gas at different locations within these disks. These maps of observed molecular abundances are confronted with our experimental findings to, first, test the validity of the ice mantle model and, second, elucidate the physical conditions in the disk, such as dust temperature and radiation dose experienced by molecules in the ice, accounting for chemical evolution and the delivery of molecules to the surrounding gas. The detection of more refractory products like COMs and the effect of warm-up of the processed ice is left for a follow-up paper. These COMs are more difficult to identify in the observations, and the more simple species are therefore better proxies of the disk evolution.

Experiments and Results

A first ice layer containing a mixture of H_2O:CH_4:NH_3 (2:1:1) was covered by a second layer composed of a CO:CH_3OH (3:1) mixture. This realistic ice sample was irradiated for 120 min with a soft X-ray spectrum covering the 250- to 1,250-eV energy range, and providing 7.6×10^{14} photons per s. The spectra of the ice during the irradiation are shown in Fig. 1, *Left*. In Fig. 1, *Right*, the column densities of CO and CH_3OH are shown, normalized to their initial values after each irradiation step.

Of the initial 156 ML of CH_3OH, only 11 ML are left after 20-min irradiation (fourth step). Thus, about 93% of the initial methanol in the ice is destroyed. In the same irradiation time, CO is reduced by 45%, from 569 ML to 312 ML. The contribution to CO and CH_3OH from the bottom layer has been estimated in an accompanying experiment performed exploiting a single layer H_2O:CH_4:NH_3 mixtures. The column densities estimated from our experiment are upper limits; as in the two-layers experiment, the radiation impinging on the bottom layer is reduced by the absorption of the top layer. Thus, the contributions to CO and CH_3OH are, at most, respectively, 4% and 10% after 20 min of irradiation, and 12% and 2% at the end of the irradiation. The CO column density also includes contribution from CH_3OH dissociation during the irradiation. In a protoplanetary disk around a T Tauri star in the region in which the temperature is ≤ 30 K (i.e., beyond 50 AU), the predicted X-ray flux is $\leq 10^{-3}$ erg·cm^{-2}·s^{-1} (23). Thus, the same amount of energy experienced by our sample in 20 min would require a time $\geq 4 \times 10^5$ y, compatible with the lifetime of circumstellar disks (24).

The steep destruction of the methanol in the top layer could be ascribed to the formation of new species and/or photodesorption. In Fig. 2 are the mass-to-charge (m/z) signals of parent molecules ($m/z = 28$ and 31 for CO and CH_3OH) and of the main products of the top layer HCO, H_2CO, and CO_2 ($m/z = 29$, 30, and 44) desorbing during the irradiation. The most intense fragment of methanol $m/z = 31$ was selected considering that $m/z = 32$ can be dominated by O_2 molecules. The largest photodesorption is detected for $m/z = 28$ related to CO. The $m/z = 29$ is larger than expected for the carbon monoxide isotopologue (^{13}CO), and it is representative of the unreacted HCO radicals detected in the infrared spectra at 1,848 cm^{-1}, or the main fragment of formaldehyde ($m/z = 30$). CO_2 is the main product photodesorbing from the top layer, and $m/z = 44$ is the second-most intense photodesorbing mass. The spectrum of $m/z = 31$ is very noisy, testifying that photodesorption of methanol is negligible and suggesting that methanol contribution to the synthesis of new species must be mainly responsible for its destruction. Methanol contribution to $m/z = 29$ is thus negligible. H_2CO ($m/z = 30$) is one of the major products of the irradiation (20, 25) of a CH_3OH ice; in Fig. 2, its photodesorption is much higher than that of the CH_3OH parent molecule.

The mass spectra in Fig. 2 show an abnormal behavior as compared to the typical X-ray photodesorption spectra in which the desorption peaks decrease monotonically during the irradiation (12, 13). In all masses, a significant increase of the desorption appears at the fourth irradiation step, suggesting a possible contribution from species produced in the bottom layer. This hypothesis has been investigated by running a second experiment in which isotopologues of methane ($^{13}CH_4$) and ammonia ($^{15}NH_3$) have been used in the bottom layer mixture.

In Fig. 3, *Top*, the spectra of $m/z = 31$ are reported for the experiments with and without isotopologues in the bottom layer. The two profiles are similar, but, from the fourth irradiation step, the bottom layer products start dominating the photodesorption. The species contributing to $m/z = 31$ in the experiment with isotopologues is formaldehyde ($H_2^{13}CO$) produced in the bottom layer. The photodesorption of formaldehyde from the bottom layer is confirmed by the comparison of $m/z =$ 30 (H_2CO) and m/z = 31 ($H_2^{13}CO$) in the experiments without and with isotopologues, shown in Fig. 3, *Bottom*. While desorption of formaldehyde from the top layer dominates the

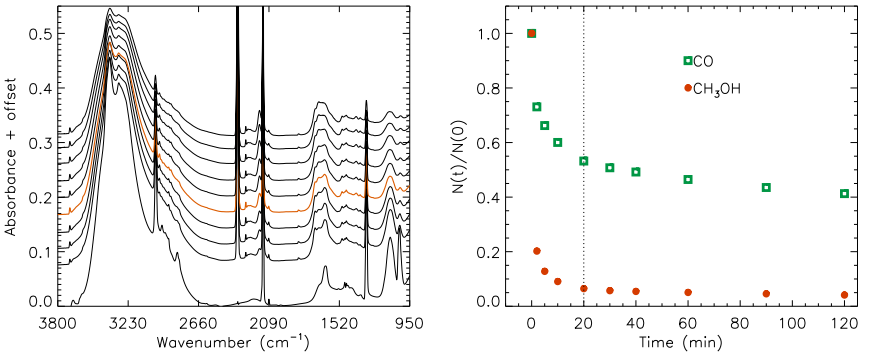

Fig. 1. (*Left*) Infrared spectra of the bilayer ice before irradiation (bottom curve) and after each irradiation step. The orange spectrum is obtained after the fourth irradiation step. The spectra have been shifted for clarity. (*Right*) Column densities of CO and CH_3OH normalized to the their initial values as functions of the irradiation time. The vertical dotted line marks the fourth irradiation step.

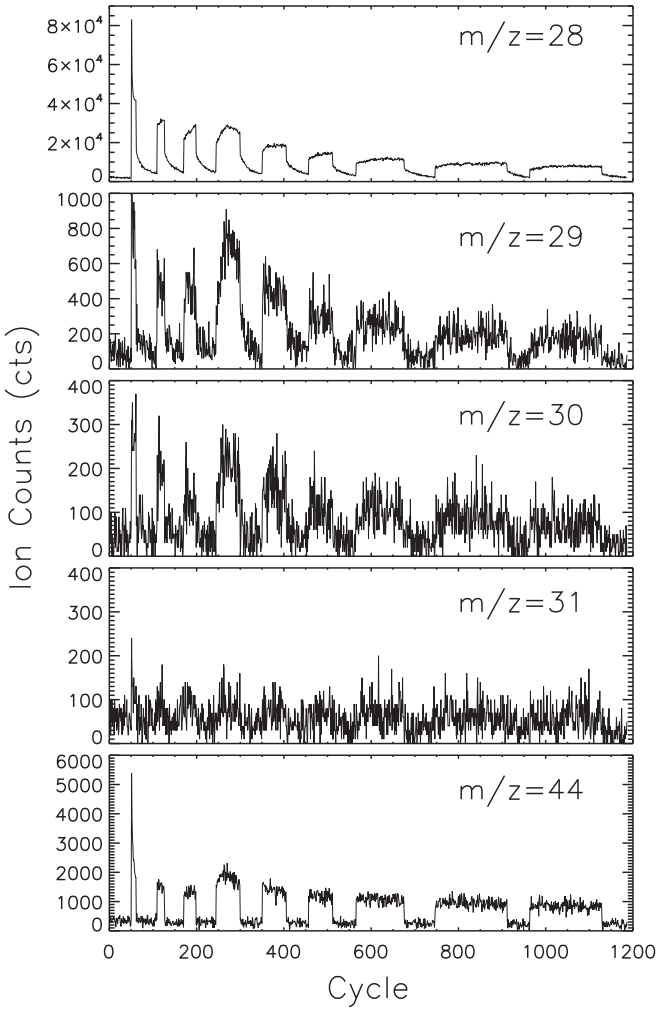

Fig. 2. Ion current vs. cycle detected by the mass spectrometer during the nine irradiation steps for the parent molecules $m/z = 28$ (CO) and m/z = 31 (CH_3OH), and for the main products of the top layer HCO, H_2CO, and CO_2 ($m/z = 29$, 30, and 44). The increase of the desorption at the fourth irradiation step marks the contribution of the bottom layer.

first three irradiation steps, the component coming from the bottom layers takes over after the fourth irradiation step. Desorption of species from the bottom layer implies that bulk diffusion occurred in the ice during irradiation. Given the small size of the X-ray spot (0.08 cm^2) as compared to the ice surface ($\sim$2 cm^2), we exclude contribution of the bottom layer from the ice edges.

Discussion and Conclusions

The penetration depth of X-rays allows processing of dust particles of a few microns. A direct outcome of this effect in X-ray experiments is the high production and release of H_2 from the dissociation of ice molecules such as H_2O and CH_3OH (12), which should contribute to the H_2 abundances observed in disks around young stars (26). Several other species were identified in circumstellar disks; these include H_2O, CO, CO_2, HCO^+, H_2CO, HCOOH, C_2H, C_2H_2, C_3H_2, CN, HCN, CH_3CN, HC_3N, N_2H^+, SO, SO_2, and CS (27–34).

It was proposed that CO is locked in ice mantles below 30 K, where it can form CH_3OH, CO_2, and/or hydrocarbons (35). H_2CO in the gas was related to a formation by hydrogenation of CO in the dust to match the disk observations (36). The detection of methanol in the cold gas of protoplanetary disks is considered a product of ice chemistry (37). The identification of CH_3OH and other complex species in FUors (FU Orionis stars) protostars (38) strongly support the role of ices in the synthesis of COMs in space. The protoplanetary disk of young Herbig Ae star HD 163296 presents a much lower methanol-to-formaldehyde ratio compared to the Class II disk of T Tauri star TW Hya. Among other possibilities, this could be attributed to differences in the stellar irradiation, uncertainties in the grain surface formation, and desorption efficiencies of CH_3OH and H_2CO (39).

In this work, we have experimentally simulated a realistically stratified ice mantle surrounding dust grains by making a double layer ice in which a mixture of H_2O:CH_4:NH_3 was covered by a second mixture of CO:CH_3OH (Fig. 4). Such an ice was irradiated with soft X-rays of energy spectrum in the range 250 eV to 1,250 eV. In the experiments, CH_3OH is rapidly converted to new species, with H_2CO, HCO, and CO being the most abundant ones. Photodesorption of CH_3OH was negligible, while a fraction of the new species was found to desorb during the X-ray irradiation at 11 K. A similar experiment using the isotopologues $^{13}CH_4$ and $^{15}NH_3$ demonstrated that photodesorption is not a surface phenomenon only. Indeed, during the irradiation ion current of mass-to-charge ratio corresponding to CO, HCO, H_2CO, and CO_2, all have contributions from bottom layer species that found their way to the surface of the ice. The obtained results can explain the nondetection of methanol in the gas toward disk regions exposed to radiation and, meanwhile, the presence of CO, HCO, and H_2CO. Other hydrogenated species like H_2O, CH_4, and NH_3 present in the first accreted ice layer are efficiently processed as well by X-rays, but their products are to a much lesser extent ejected to the gas. In this experiment, desorption of species from the bottom layer is detected, implying that bulk diffusion occurred during X-ray irradiation. Bulk diffusion is highly relevant for the formation of complex species in ice mantles, and has received attention both theoretically (40, 41) and experimentally (42, 43). A detailed analysis of

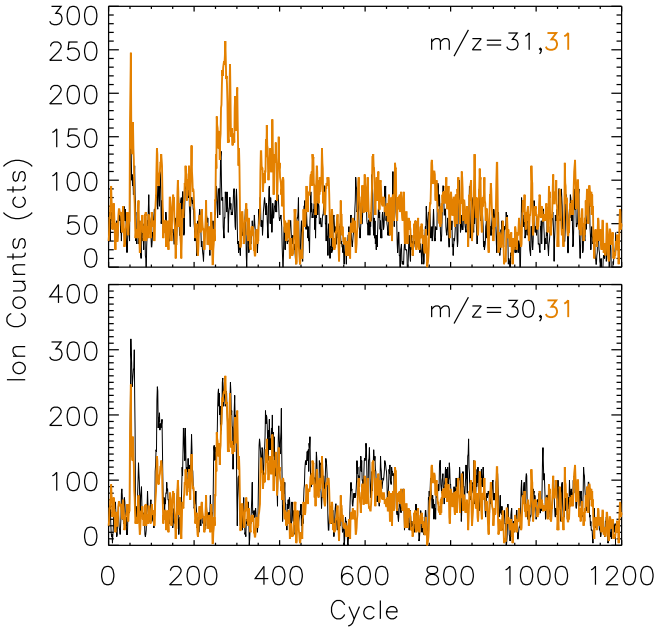

Fig. 3. (*Top*) Mass spectra of $m/z = 31$ with (orange) and without (black) isotopologues. From the fourth irradiation step, the desorption of $H_2^{13}CO$ is detected. (*Bottom*) Comparison of $m/z = 30$ (H_2CO) and m/z = 31 ($H_2^{13}CO$) in the experiments without and with isotopologues.

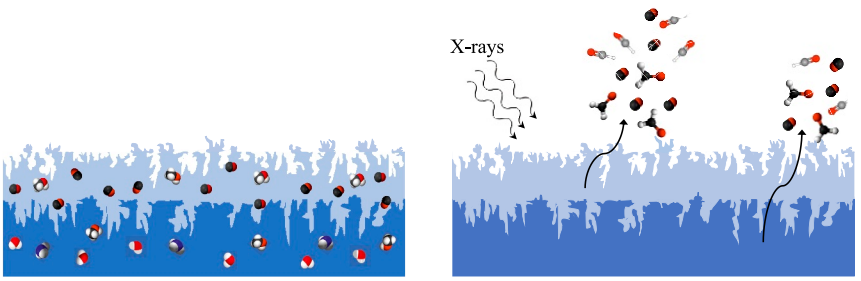

Fig. 4. Sketch of the bilayer ice experiment. (*Left*) The bottom H_2O:CH_4:NH_3 (2:1:1) mixture covered by a layer of CO:CH_3OH (3:1). (*Right*) X-ray irradiation of the ice induces a very fast destruction of CH_3OH, leading to the formation of new species rather than its photodesorption. During the irradiation, a negligible desorption of CH_3OH has been detected, while CO and products such as HCO, H_2CO, and CO_2 show the most intense desorption signals. Desorption from the bottom layer species was also detected.

the bulk diffusion in the present experiments is beyond the scope of this work, and we defer a detailed analysis to a dedicated paper.

In summary, the absence or low abundance of complex species from the cold gas in protoplanetary disks, and the presence of abundant CO, HCO, and H_2CO and negligible CH_3OH is compatible with the X-ray processing of realistic ice mantles in the disks around young stars. Moreover, the experimental simulations are also compatible with low abundances of other COMs in the cold parts of the disk, since they are formed in the ice bulk but are not ejected into the gas phase.

Methods

The experiments were performed with the Interstellar Energetic-Process System (44) ultra-high vacuum chamber at a base pressure of $< 5 \times 10^{-10}$ mbar. The chamber is equipped with a Quadrupole Mass Spectrometer (QMS) and a midinfrared spectrometer. This setup was connected to the BL08B soft X-ray beamline at National Synchrotron Radiation Research Center (NSRRC, Taiwan), providing a flux of 7.6×10^{14} photons per s covering the energy range 250 eV to 1,250 eV. The ice was made of a H_2O:CH_4:NH_3 (2:1:1) mixture covered by a top layer of CO:CH_3OH (3:1) mixture deposited onto a CaF_2 substrate at 12 K, which allowed infrared spectroscopy of the ice samples in transmittance. H_2O is from Merck, LC MS (liquid chromatography–mass spectrometry) grade; CH_4 is from Matheson TRI- GAS 99.999%, NH_3 is from Specialty Gases of America, 99.99%; CO is from Cingfong Gas Industrial, purity 99.99%; and CH_3OH is from Merck, 99.9%. A similar experiment with a bottom layer made of H_2O:$^{13}CH_4$:$^{15}NH_3$ was also performed. The $^{13}CH_4$ is from Specialty Gases of America, ^{13}C atom 99%; and $^{15}NH_3$ is from Cambridge Isotope Laboratories, Inc., 98% atom ^{15}N. The QMS was used for monitoring the gas-phase components in the chamber during deposition and the desorbing molecules during irradiation. The ice samples were irradiated in nine steps (2, 3, 5, 10, 10, 10, 20, 30, and 30 min) for a total of 120 min. At the end of each step, infrared spectra were collected. The ice column density was computed as the sum of bottom $N_{H_2O} + N_{CH_4} + N_{NH_3}$ and top $N_{CO} + N_{CH_3OH}$ layers from integration of the bands using the expression

$$N = \frac{1}{A} \int_{band} \tau_\nu d\nu, \quad [1]$$

where N is the column density in molecules per square centimeter, τ_ν is the optical depth of the band, $d\nu$ is the wavenumber differential in per centimeter, and A is the band strength in centimeters per molecule. The integrated absorbance is $0.43 \times \tau$, where τ is the integrated optical depth of the band. In the ice sample without isotopologues, the bottom ($N_{H_2O} + N_{CH_4} + N_{NH_3}$) and the top ($N_{CO} + N_{CH_3OH}$) layers were 1,646 and 725 ML, respectively. In the ice sample with isotopologues, the bottom ($N_{H_2O} + N_{^{13}CH_4} + N_{^{15}NH_3}$) and the top ($N_{CO} + N_{CH_3OH}$) layers were 1,725 and 775 ML, respectively. The column density of H_2O was computed from the band at 3,280 cm^{-1} and a band strength of 2.0×10^{-16} cm per molecule (45). The band at 1,304 cm^{-1} and a band strength of 8.0×10^{-18} cm per molecule were used for N_{CH_4} (46). Ammonia N_{NH_3} was computed using the feature at 1,112 cm^{-1} and a band strength of 1.7×10^{-17} cm per molecule (47). The column density of carbon monoxide was obtained by integration of the band at 2,138 cm^{-1} and a band strength of 1.1×10^{-17} cm per molecule (48). Methanol N_{CH_3OH} was computed using the feature at 1,026 cm^{-1} and a band strength of 1.8×10^{-17} cm per molecule (49).

Data of this work are available at Harvard Dataverse (DOI: 10.7910/DVN/TMB6AF).

ACKNOWLEDGMENTS. We acknowledge the NSRRC general staff for running the synchrotron radiation facility. We also thank Dr. T.-W. Pi, the spokesperson of BL08B in NSRRC. The Spanish Ministry of Science, Innovation and Universities supported this research under Grant AYA2017-85322-R (Agencia Estatal de Investigación/ European Funds, European Union), and Program MDM-2017-0737 Unidad de Excelencia "María de Maeztu"–Centro de Astrobiología (Instituto Nacional de Técnica Aerospacial, Consejo Superior de Investigaciones Científicas). We also acknowledge support from the PRIN-INAF 2016 The Cradle of Life - GENESIS-SKA, the MOST Grant MOST 107-2112-M-008-016-MY3 from Taiwan, and ASI-INAF n.2018-16-HH.0, Project "SPACE Tweezers."

1. E. Dartois, The ice survey opportunity of ISO. *Space Sci. Rev.* **119**, 293–310 (2005).
2. K. I. Öberg *et al.*, The *Spitzer* ice legacy: Ice evolution from cores to protostars. *Astrophys. J.* **740**, 109 (2011).
3. A. C. A. Boogert, P. A. Gerakines, D. C. B. Whittet, Observations of the icy universe. *Annu. Rev. Astron. Astrophys.* **53**, 541–581 (2015).
4. E. M. Penteado *et al.*, Spectroscopic constraints on CH_3OH formation: CO mixed with CH_3OH ices towards young stellar objects. *Mon. Not. Roy. Astron. Soc.* **454**, 531–540 (2015).
5. N. Watanabe, A. Kouchi, Efficient formation of formaldehyde and methanol by the addition of hydrogen atoms to CO in H_2O-CO ice at 10 K. *Astrophys. J. Lett.* **571**, L173–L176 (2002).
6. K. I. Oberg, Photochemistry and astrochemistry: Photochemical pathways to interstellar complex organic molecules. *Chem. Rev.* **116**, 9631–9663 (2016).
7. G. M. Muñoz Caro *et al.*, Amino acids from ultraviolet irradiation of interstellar ice analogues. *Nature* **416**, 403–406 (2002).
8. M. P. Bernstein, J. P. Dworkin, S. A. Sandford, G. W. Cooper, L. J. Allamandola, Racemic amino acids from the ultraviolet photolysis of interstellar ice analogues. *Nature* **416**, 401–403 (2002).
9. C. Meinert *et al.*, Ribose and related sugars from ultraviolet irradiation of interstellar ice analogs. *Science* **352**, 208–212 (2016).
10. Y. Oba, Y. Takano, H. Naraoka, N. Watanabe, A. Kouchi, Nucleobase synthesis in interstellar ices. *Nat. Commun.* **10**, 4413 (2019).
11. Z. Kaòuchová *et al.*, Synthesis of formamide and isocyanic acid after ion irradiation of frozen gas mixtures. *Astron. Astrophys.* **585**, A155 (2016).
12. A. Jiménez-Escobar *et al.*, X-ray photo-desorption of H_2O:CO:NH_3 circumstellar ice analogs: Gas-phase enrichment. *Astrophys. J.* **868**, 73 (2018).
13. A. Ciaravella *et al.*, Synthesis of complex organic molecules in soft X-ray irradiated ices. *Astrophys. J.* **879**, 21 (2019).
14. A. G. G. M. Tielens, A. T. Tokunaga, T. R. Geballe, F. Baas, Interstellar solid CO: Polar and nonpolar interstellar ices. *Astrophys. J.* **381**, 181 (1991).
15. K. M. Pontoppidan *et al.*, The c2d *Spitzer* spectroscopic survey of ices around low-mass young stellar objects. II. CO_2. *Astrophys. J.* **678**, 1005–1031 (2008).
16. G. M. Muñoz Caro, W. A. Schutte, UV-photoprocessing of interstellar ice analogs: New infrared spectroscopic results. *Astron. Astrophys.* **412**, 121–132 (2003).
17. P. de Marcellus *et al.*, Photo and thermochemical evolution of astrophysical ice analogues as a source for soluble and insoluble organic materials in Solar system minor bodies. *Mon. Not. Roy. Astron. Soc.* **464**, 114–120 (2017).
18. P. A. Gerakines *et al.*, Observations of solid carbon dioxide in molecular clouds with the *Infrared Space Observatory*. *Astrophys. J.* **522**, 357–377 (1999).
19. E. Dartois *et al.*, Methanol: The second most abundant ice species towards the high-mass protostars RAFGL7009S and W 33A. *Astron. Astrophys.* **342**, L32–L35 (1999).

20. K. I. Öberg, R. T. Garrod, E. F. van Dishoeck, H. Linnartz, Formation rates of complex organics in UV irradiated CH_3OH-rich ices. I. Experiments. *Astron. Astrophys.* **504**, 891–913 (2009).
21. G. M. Muñoz Caro *et al.*, X-ray versus ultraviolet irradiation of astrophysical ice analogs leading to formation of complex organic molecules. *ACS Earth Space Chem.* **3**, 2138–2157 (2019).
22. I. Ribas, E. F. Guinan, M. Güdel, M. Audard, Evolution of the solar activity over time and effects on planetary atmospheres. I. high-energy irradiances (1-1700 Å). *Astrophys. J.* **622**, 680–694 (2005).
23. C. Walsh, H. Nomura, T. J. Millar, Y. Aikawa, Chemical processes in protoplanetary disks. II. On the importance of photochemistry and X-ray ionization. *Astrophys. J.* **747**, 114 (2012).
24. A. J. W. Richert *et al.*, Circumstellar disc lifetimes in numerous galactic young stellar clusters. *Mon. Not. Roy. Astron. Soc.* **477**, 5191–5206 (2018).
25. Y. J. Chen *et al.*, Soft X-ray irradiation of methanol ice: Formation of products as a function of photon energy. *Astrophys. J.* **778**, 162 (2013).
26. T. L. Beck, J. S. Bary, A search for spatially resolved infrared rovibrational molecular hydrogen emission from the disks of young stars. *Astrophys. J.* **884**, 159 (2019).
27. F. Lahuis *et al.*, Hot organic molecules toward a young low-mass star: A look at inner disk chemistry. *Astrophys. J. Lett.* **636**, L145–L148 (2006).
28. C. Qi, K. I. Öberg, D. J. Wilner, K. A. Rosenfeld, First detection of c-C_3H_2 in a circumstellar disk. *Astrophys. J. Lett.* **765**, L14 (2013).
29. K. I. Öberg *et al.*, The comet-like composition of a protoplanetary disk as revealed by complex cyanides. *Nature* **520**, 198–201 (2015).
30. L. Podio *et al.*, The jet and the disk of the HH 212 low-mass protostar imaged by ALMA: SO and SO_2 emission. *Astron. Astrophys.* **581**, A85 (2015).
31. M. T. Carney *et al.*, Increased H_2CO production in the outer disk around HD 163296. *Astron. Astrophys.* **605**, A21 (2017).
32. C. Favre *et al.*, First detection of the simplest organic acid in a protoplanetary disk. *Astrophys. J. Lett.* **862**, L2 (2018).
33. A. S. Booth *et al.*, Sulphur monoxide exposes a potential molecular disk wind from the planet-hosting disk around HD 100546. *Astron. Astrophys.* **611**, A16 (2018).
34. A. S. Booth, C. Walsh, J. D. Ilee, First detections of $H^{13}CO^+$ and $HC^{15}N$ in the disk around HD 97048. Evidence for a cold gas reservoir in the outer disk. *Astron. Astrophys.* **629**, A75 (2019).
35. A. D. Bosman, C. Walsh, E. F. van Dishoeck, CO destruction in protoplanetary disk midplanes: Inside versus outside the CO snow surface. *Astron. Astrophys.* **618**, A182 (2018).
36. L. Podio *et al.*, Organic molecules in the protoplanetary disk of DG Tauri revealed by ALMA. *Astron. Astrophys.* **623**, L6 (2019).
37. C. Walsh *et al.*, First detection of gas-phase methanol in a protoplanetary disk. *Astrophys. J. Lett.* **823**, L10 (2016).
38. J.-E. Lee *et al.*, The ice composition in the disk around V883 Ori revealed by its stellar outburst. *Nat. Astron.* **3**, 314–319 (2019).
39. M. T. Carney *et al.*, Upper limits on CH_3OH in the HD 163296 protoplanetary disk. Evidence for a low gas-phase CH_3OH-to-H_2CO ratio. *Astron. Astrophys.* **623**, A124 (2019).
40. H. M. Cuppen *et al.*, Grain surface models and data for astrochemistry. *Space Sci. Rev.* **212**, 1–58 (2017).
41. P. Ghesquière *et al.*, Diffusion of molecules in the bulk of a low density amorphous ice from molecular dynamics simulations. *Phys. Chem. Chem. Phys.* **17**, 11455–11468 (2015).
42. F. Mispelaer *et al.*, Diffusion measurements of CO, HNCO, H_2CO, and NH_3 in amorphous water ice. *Astron. Astrophys.* **555**, A13 (2013).
43. P. Ghesquière, A. Ivlev, J. A. Noble, P. Theulé, Reactivity in interstellar ice analogs: Role of the structural evolution. *Astron. Astrophys.* **614**, A107 (2018).
44. C. H. Huang *et al.*, Effects of 150-1000 eV electron impacts on pure carbon monoxide ices using the interstellar energetic-process system (IEPS). *Astrophys. J.* **889**, 57 (2020).
45. P. A. Gerakines, W. A. Schutte, J. M. Greenberg, E. F. van Dishoeck, The infrared band strengths of H_2O, CO and CO_2 in laboratory simulations of astrophysical ice mixtures. *Astron. Astrophys.* **296**, 810–818 (1995).
46. M. Bouilloud *et al.*, Bibliographic review and new measurements of the infrared band strengths of pure molecules at 25 K: H_2O, CO_2, CO, CH_4, NH_3, CH_3OH, HCOOH and H_2CO. *Mon. Not. Roy. Astron. Soc.* **451**, 2145–2160 (2015).
47. S. A. Sandford, L. J. Allamandola, Condensation and vaporization studies of CH 3OH and NH 3 ices: Major implications for astrochemistry. *Astrophys. J.* **417**, 815 (1993).
48. G. J. Jiang, W. B. Person, K. G. Brown, Absolute infrared intensities and band shapes in pure solid CO and CO in some solid matrices. *J. Chem. Phys.* **62**, 1201–1211 (1975).
49. P. A. Gerakines, W. A. Schutte, P. Ehrenfreund, Ultraviolet processing of interstellar ice analogs. I. Pure ices. *Astron. Astrophys.* **312**, 289–305 (1996).